5660 *Chem. Mater.* **2010,** *22,* 5660–5666
DOI:10.1021/cm1019603

CHEMISTRY OF MATERIALS
Article

Synthesis of Atomically Thin WO_3 Sheets from Hydrated Tungsten Trioxide

Kourosh Kalantar-zadeh,*[,†,‡] Aravind Vijayaraghavan,[†] Moon-Ho Ham,[†] Haidong Zheng,[‡] Michael Breedon,[‡] and Michael S. Strano[†]

[†]*Department of Chemical Engineering, Massachusetts Institute of Technology, Cambridge, Massachusetts 02139, and* [‡]*School of Electrical and Computer Engineering, RMIT University, Melbourne, Victoria 3001*

Received July 15, 2010. Revised Manuscript Received August 22, 2010

Atomically thin WO_3 is fabricated using a three-step process, involving wet-chemical synthesis of hydrated-WO_3, mechanical exfoliation of fundamental layers and dehydration by annealing at 300 °C. Atomic force microscopy reveals that the minimum resolvable thickness of the hydrated flakes to be ~1.4 nm, which corresponds to the unit-cell height. The subsequent annealing temperature determines the degree of dehydration and thereby the crystallographic structure of the resultant WO_3. The hydrated and dehydrated flakes are characterized by Raman spectroscopy to reveal spectroscopic fingerprints of flake thickness. Thin flakes are also shown to have higher propensity for lithium intercalation, which is also evidenced in Raman planar peak intensity.

Introduction

Properties of metal oxides are known to be strongly dependent on parameters such as morphology, crystal phase, oxygen deficiency, and doping.[1] By reducing the metal oxides' dimensions, it is possible to tailor their electronic and optical characteristics, and subsequently tune their properties for targeted applications.[2] Using different exfoliation techniques, it is possible to reduce the thickness of stratified metal oxides in one dimension and form quasi two-dimensional (2D) nano sheets.[3,4] In such 2D sheets, the reduced third dimension leads to confinement and quantization of electrons and phonons, altering the photon-exciton conversion rate, the electron−phonon interaction behaviors and the free carrier lifetime. Additionally, these sheets are stable down to nanometer dimensions.[5] Because of such qualities, the metal oxide sheets can be ultimately used as building blocks for the fabrication of unique devices such as fast switches, field effect transistors with large transconductance, fast photo- and electrochromic transducers, highly sensitive detectors, and optical modulators.[6−10] Using such nanosheets, it is possible to tailor superlattice assemblies, quantum wells, and sophisticated heterostructures with unique electronic and magnetic propeties.[10−14]

In this work, we will demonstrate the formation of nanosheets consisting of atomically thin WO_3 fundamental layers. For the development of functional electronic and optical devices, WO_3 is an ideal choice. Its bandgap can be tuned in the range of 2.5−3.7 eV by structural manipulations and doping,[15,16] and can also be formed into nanostructued thin films via a variety of liquid based processes such as anodization,[17−22] and colloidal chemical methods,[23] as well as gaseous phase processes such as thermal evaporation[24] and sputtering.[25] WO_3 has received

*Corresponding author. E-mail: kourosh.kalantar@rmit.edu.au and kourosh@mit.edu.

(1) Chambers, S. A. *Adv. Mater.* **2010**, *22*, 219.
(2) Kalantar-zadeh, K.; Fry, B. *Nanotechology Enabled Sensors*; Springer: Boston, 2007.
(3) Kalantar-zadeh, K.; Tang, J.; Wang, M.; Wang, K. L.; Shailos, A.; Galatsis, K.; Kojima, R.; Strong, V.; Lech, A.; Wlodarski, W.; Kaner, R. B. *Nanoscale* **2010**, *2*, 429.
(4) Sasaki, T. *J. Ceram. Soc. Jpn.* **2007**, *115*, 9.
(5) Osada, M.; Ebina, Y.; Funakubo, H.; Yokoyama, S.; Kiguchi, T.; Takada, K.; Sasaki, T. *Adv. Mater.* **2006**, *18*, 1023.
(6) Keller, S. W.; Kim, H. N.; Mallouk, T. E. *J. Am. Chem. Soc.* **1994**, *116*, 8817.
(7) Zhou, Y.; Ma, R. Z.; Ebina, Y.; Takada, K.; Sasaki, T. *Chem. Mater.* **2006**, *18*, 1235.
(8) Schaak, R. E.; Mallouk, T. E. *Chem. Mater.* **2000**, *12*, 2513.
(9) Schaak, R. E.; Mallouk, T. E. *Chem. Mater.* **2002**, *14*, 1455.
(10) Chen, S. J.; Liu, Y. C.; Shao, C. L.; Mu, R.; Lu, Y. M.; Zhang, J. Y.; Shen, D. Z.; Fan, X. W. *Adv. Mater.* **2005**, *17*, 586.
(11) Osada, M.; Ebina, Y.; Takada, K.; Sasaki, T. *Adv. Mater.* **2006**, *18*, 295.
(12) Sato, H.; Ono, K.; Sasaki, T.; Yamagishi, A. *J. Phys. Chem. B* **2003**, *107*, 9824.
(13) Osada, M.; Sasaki, T. *J. Mater. Chem.* **2009**, *19*, 2503.
(14) Felser, C.; Fecher, G. H.; Balke, B. *Angew. Chem., Int. Ed.* **2007**, *46*, 668.
(15) Barton, D. G.; Shtein, M.; Wilson, R. D.; Soled, S. L.; Iglesia, E. *J. Phys. Chem. B* **1999**, *103*, 630.
(16) Deb, S. K. *Solar Energy Mater. & Solar Cells* **2008**, *92*, 245.
(17) Hahn., R.; Macak, J. M.; Schmuki, P. *Electrochem. Commun.* **2007**, *9*, 947.
(18) Tsuchiya, H.; Macak, J. M.; Sieber, I.; Taveira, L; Ghicov, A.; Sirotna, K.; Schmuki, P. *Electrochem. Commun.* **2005**, *7*, 295.
(19) de Tacconi, N. R.; Chenthamarakshan, C. R.; Yogeeswaran, G.; Watcharenwong, A.; de Zoysa, R. S.; Basit, N. A; Rajeshwar, K. *J. Phys. Chem. B* **2006**, *110*, 25347.
(20) Watcharenwong, A.; Chanmanee, W.; de Tacconi, N. R.; Chenthamarakshan, C. R.; Kajitvichyanukul, P.; Rajeshwar, K. *J. Electroanal. Chem.* **2008**, *612*, 112.
(21) Nah, Y. C.; Ghicov, A.; Kim, D.; Schmuki, P. *Electrochem. Commun.* **2008**, *10*, 1777.
(22) Yang, M.; Shrestha, N. K.; Schmuki, P. *Electrochem. Commun.* **2009**, *11*, 1908.
(23) Xia, H. J.; Wang, Y.; Kong, F. H.; Wang, S. R.; Zhu, B. L; Guo, X. Z.; Zhang, J.; Wang, Y. M.; Wu, S. H. *Sens. Actuators, B* **2008**, *134*, 133.
(24) Baek, Y.; Yong, K *J. Phys. Chem.* **2007**, *111*, 1213.
(25) Yaacob, M. H.; Breedon, M.; Kalantar-Zadeh, K.; Wlodarski, W. *Sens. Actuators, B* **2009**, *137*, 115.

Published on Web 09/07/2010

surprisingly little attention despite the facts that it can produce much larger photocurrents[26] and higher photocurrent conversion efficiency[27,28] than metal oxides such as ZnO and TiO_2.[29−31] WO_3 is an intrinsic n-type semiconducting metal oxide, capable of withstanding low pH environments and high temperatures, making it an excellent choice for robust, nanostructured, inorganic frameworks.[15,32] WO_3 has been demonstrated to have applications in smart windows and flat-panel displays.[33] Additionally, there are many reports on WO_3 for a wide variety of applications in optoelectronics,[34] microelectronics,[35] catalysis,[36] and water splitting.[37] Additionally, WO_3 finds potential applications in optical memories,[38] and as chemical sensors.[25,39,40]

Mechanical exfoliation technique will be used for obtaining nanosheets of WO_3 from layered hydrated metal oxide, which in turn will be obtained using a wet chemical route. We will show that these stratified hydrated WO_3, which is made of planes bonded together by weak Van der Waal forces, can be exfoliated at their week bonds by mechanical forces. Depending on the initial phase of the hydrated WO_3 obtained in the wet process, the degree of hydration, and the annealing procedure, the resulting tungsten oxide can be monoclinic, hexagonal, or orthorhombic with different degrees of oxidation.[41] We will confirm that by using the mechanical exfoliation technique, the layered WO_3 can be thinned down into fundamental layers. The thicknesses of obtained nanosheets increase at the unique step magnitude of ~1.4 nm, which is equal to this unit-cell height. Unlike the case of graphene, little attention has been paid to the correlation between number of layers and properties of metal oxides. Here, the vibrational information of the exfoliated sheets of different thicknesses after exposure to intercalating ions and atoms will be presented and compared via Raman spectroscopy. These experiments highlight the advantage of reducing the number of layers to obtain atomically thick sheets consisting of fundamental layers of WO_3.

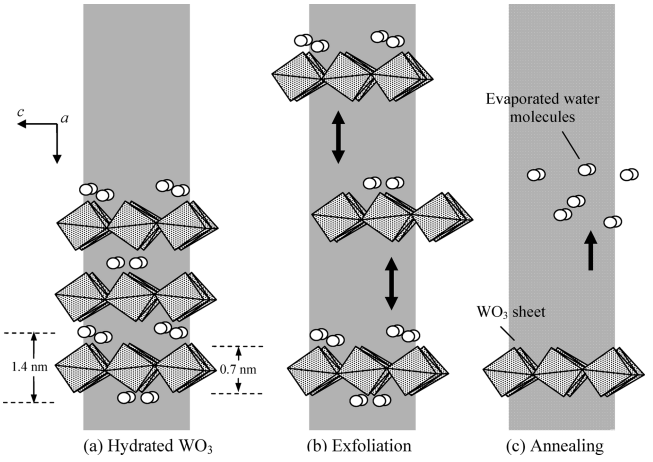

Figure 1. Schematic of the formation of single layer of monoclinic WO_3 from layered hydrated WO_3 via an exfoliation process: (a) hydrated WO_3 ($WO_3.2H_2O$), which is made of layers of WO_3 with H_2O molecules in between layers; (b) mechanical exfoliation separate layers at their weakest bonds into 1.4 nm sheets, and (c) water molecules are evaporated and WO_3 layers of multiples of 0.7 nm thickness are formed.

Formation of Atomically Thin Sheets

The mechanical exfoliation route employed here has gained recent prominence in the fabrication of atomically thin sheets of graphene.[42,43] This method can also be applied to exfoliate other layered materials, which have strong in-plane atomic bonds and weak interlayer bonds. Many metal oxides, such as MoO_3, V_2O_5, and hydrated WO_3, have such layered crystallographic phases that can therefore be mechanically exfoliated.[3]

No layered dehydrated WO_3 crystals are known. As a result, the best starting material for mechanical exfoliation is hydrated WO_3, which can be synthesized in layered and highly ordered forms (Figure 1).[32,41] These qualities are the necessary initial conditions for mechanical exfoliation in order to obtain perfect sheets of nanometer thicknesses. Wet-chemical synthesis routes of WO_3 generally result in stratified structures, which are highly crystalline across the planes and contain H_2O between the layers. The water content in the hydrated WO_3 appears to be very crucial in the stabilization of different types of WO_3 crystal phases after annealing.[41] The best starting material for exfoliation is $WO_3.2H_2O$ which exhibits a layered structure (a = 10.484 Å, b = 13.804 Å, c = 10.573 Å) with weak van der Waals bonds between planes, because the distance between adjacent planes is 0.7 nm, which is larger than other less hydrated WO_3 forms. It consists of a corner-sharing single sheets of $WO_5(OH_2)$, and a second water molecule, which is placed between the interlayers (Figure 1).

We used a wet synthesis method to produce hydrated stratified WO_3 by placing pieces of tungsten foil (99.9+%, Aldrich) in a reaction flask of 0.5 M HNO_3. The flask was kept at 80 °C for 6 h until yellow thin films completely

(26) Zhang, J. G.; Benson, D. K.; Tracy, C. E.; Deb, S. K.; Czanderna, A. W.; Bechinger, C. *J. Electrochem. Soc.* **1997**, *144*, 2022.
(27) Berger, S.; Tsuchiya, H.; Ghicov, A.; Schmuki, P. *Appl. Phys. Lett.* **2006**, *88*, 203119.
(28) Nah, Y. C.; Paramasivam, I.; Hahn, R.; Shrestha, N. K.; Schmuki, P. *Nanotechnology* **2010**, *21*, 105704.
(29) Sadek, A. Z.; Zheng, H. D.; Breedon, M.; Bansal, V.; Bhargava, S. K.; Latham, K.; Zhu, J. M.; Yu, L. S.; Hu, Z.; Spizzirri, P. G.; Wlodarski, W.; Kalantar-zadeh, K. *Langmuir* **2009**, *25*, 9545.
(30) Zheng, H. D.; Sadek, A. Z.; Latham, K.; Kalantar-Zadeh, K. *Electrochem. Commun.* **2009**, *11*, 768.
(31) Ghicov, A.; Schmuki, P. *Chem. Commun.* **2009**, *20*, 2791.
(32) Breedon, M.; Spizzirri, P.; Taylor, M.; du Plessis, J.; McCulloch, D.; Zhu, J. M.; Yu, L. S.; Hu, Z.; Rix, C.; Wlodarski, W.; Kalantar-zadeh, K. *Cryst. Growth Des.* **2010**, *10*, 430.
(33) Rougier, A.; Portemer, F.; Quede, A.; El Marssi, M. *Appl. Surf. Sci.* **1999**, *153*, 1.
(34) Granqvist, C. G. *Sol. Energy Mater. Sol. Cells* **2000**, *60*, 201.
(35) Sun, M.; Xu, N.; Cao, Y. W.; Yao, J. N.; Wang, E. G. *J. Mater. Res.* **2000**, *15*, 927.
(36) Yagi, M.; Maruyama, S.; Sone, K.; Nagai, K.; Norimatsu, T. *J. Solid State Chem.* **2008**, *181*, 175.
(37) Fujishima, A.; Honda, K. *Nature* **1972**, *238*, 37.
(38) Takeda, Y.; Kato, N.; Fukano, T.; Takeichi, A.; Motohiro, T.; Kawai, S. *J. Appl. Phys.* **2004**, *96*, 2417.
(39) Qu, W. M.; Wlodarski, W. *Sens. Actuators, B* **2000**, *64*, 42.
(40) Penza, M.; Martucci, C.; Cassano, G. *Sens. Actuators, B* **1998**, *50*, 52.
(41) Kuti, L. M.; Bhella, S. S.; Thangadurai, V. *Inorg. Chem.* **2009**, *48*, 6804.
(42) Novoselov, K. S.; Geim, A. K.; Morozov, S. V.; Jiang, D.; Zhang, Y.; Dubonos, S. V.; Grigorieva, I. V.; Firsov, A. A. *Science* **2004**, *306*, 666.
(43) Novoselov, K. S.; Jiang, D.; Schedin, F.; Booth, T. J.; Khotkevich, V. V.; Morozov, S. V.; Geim, A. K. *Proc. Natl. Acad. Sci. U.S.A.* **2005**, *102*, 10451.

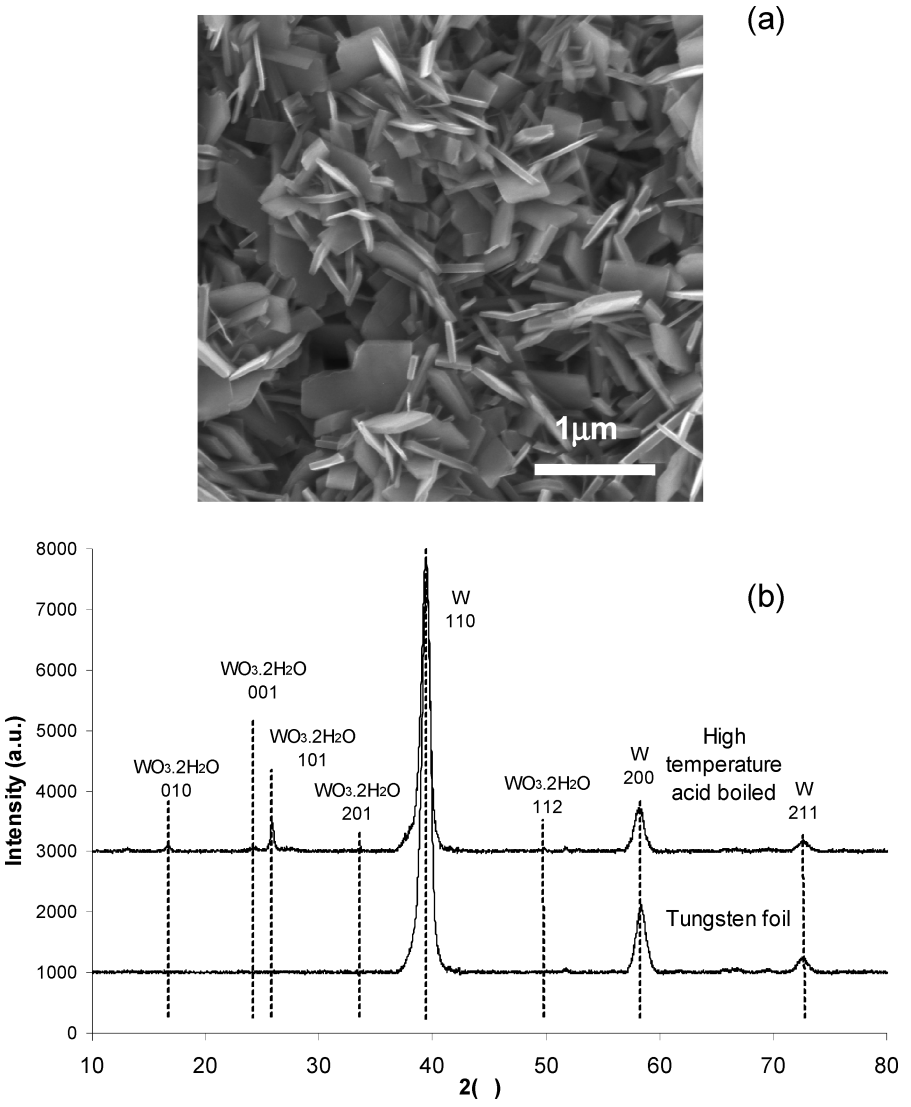

Figure 2. (a) SEM of the surface of the W foil after acid boiling, (b) XRD of the foil and the hydrated WO_3 layer made of plates.

covered their surfaces. These yellow films are made of hydrated WO_3 platelets. The scanning electron microscope (SEM) image (taken by FEI Nova NanoSEM) in Figure 2a shows the morphology of the hydrated WO_3 films. Randomly oriented square and rectangular shaped platelets with lengths of 0.2−2 μm were observed. The thicknesses of the platelets were in the order of 40−100 nm. It was also observed that many of the platelets were aligned normal to the substrates' surfaces.

X-ray diffraction (XRD) analysis was carried out on a Bruker D8 Discover microdiffractometer fitted with a GADDS (general area detector diffraction system). Data were collected at room temperature using Cu Kα radiation (λ = 1.541, 78 Å) with a potential of 40 kV and a current of 40 mA, and filtered with a graphite monochromator in the parallel mode (175 mm collimator with 0.5 mm pinholes). The XRD patterns of the W foil before and after acid boiling (Figure 2a) are shown in Figure 2b. After annealing, in addition to strong W peaks, the hydrotungstate signatures (ICDD no. 20−1324) of $WO_3 \cdot 2H_2O$ are also seen. . The enhanced 101 reflection suggests a preferential orientation of the (101) crystal planes, which ensures that most of the platelets possess a reduced dimension in the direction normal to the substrate.

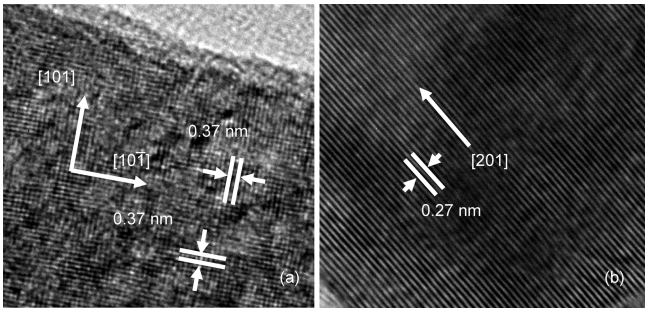

Figure 3. HRTEM of the (a) nonannealed $WO_3 \cdot 2H_2O$ and (b) annealed WO_3.

The high-resolution transmission electron microscope (HRTEM) images of the platelets before and after annealing at 300 °C are shown in Figure 3. Samples for HRTEM were prepared by sonicating the films for 1 h in DI water and subsequently drop-casting the sonicated samples onto a Cu TEM grid. TEM images were obtained using a Jeol 2010 TEM. The HRTEM image of a hydrated

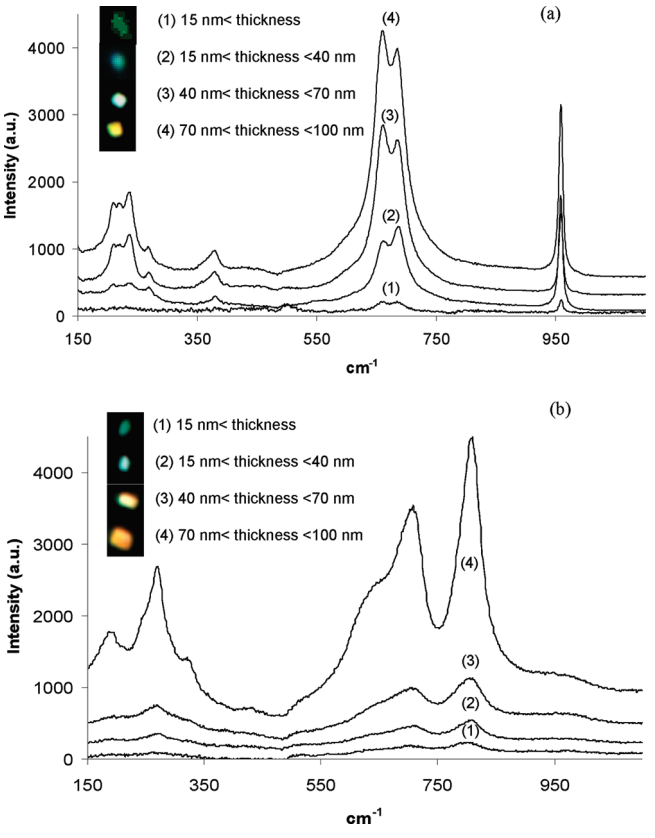

Figure 4. Raman spectra for $WO_3.2H_2O$ for samples with the thickness of several fundamental sheets (less than 15 nm) to 100 nm. Optical images of these samples are shown in the left side: (a) nonannealed samples, (b) annealed at 300 °C (inset figure width 2 μm).

WO_3 platelet in Figure 3a reveals a clear 2D crystal lattice, the interplanar distances of 0.37 nm. Selected area electron diffraction pattern (not shown) indicated the presence of the $WO_3 \cdot 2H_2O$ 101 and $10\bar{1}$ crystal planes.[44−46] The TEM image of the edge of a WO_3 platelet after annealing at 300 °C, is shown in Figure 3 (b). Refinement of crystallinity in hydrated samples after annealing can be clearly observed from the lattice fringes. The ordered lattice structure confirms that the obtained WO_3 nanoplatelet exists as a single crystal. The measured *d*-spacing of 0.27 nm can be assigned to the (201) planes of monoclinic WO_3.[45,47]

Mechanical exfoliation was carried out similar to the method initially used by Geim et al. for exfoliating graphene.[42,43] The W substrates with hydrated WO_3 films were placed on a piece of adhesive tape. The mechanical exfoliation using this tape was repeated several times until only a faint reflection of the hydrated WO_3 layer could be observed. The films were then transferred to fused quartz substrates and the tape was peeled off. Fused quartz substrates were oxygen plasma treated prior to the process to increase the adhesion of platelets onto the surface. Platelets of different colors were observed on the surface using an optical microscope under white-light illumination.

The thinnest plates were less than 15 nm and had a faint blue appearance. The platelets colors (as can be seen in Figure 4(a)) changed in the following order as a function of thickness: faint blue (< 15 nm), white (15−40 nm), yellow (40−70 nm), orange (70−100 nm), and red (100−150 nm).

Raman Investigation of Sheets

Similar to graphene, Raman spectroscopy is ideally suited for the analysis of atomically thin layers. Extracting crystallographic information using methods such as XRD, given the low dimensionality of the atomically thin layers, is largely unsuitable. Both hydrated and dehydrated WO_3 layers have strong Raman modes, which can be matched to the hydration level and crystal phase signatures. Raman spectroscopy was conducted on sheets of different thicknesses to assess the influence of both thinning and annealing process on Raman vibrational signatures typically manifesting as symmetric features as well as chemical bonds that occur during annealing. Results for the series of hydrated exfoliated WO_3 of different thicknesses are shown in Figure 4a. Micro-Raman measurements were performed on a spectrometer in a backscattering geometry, excited by a 632 nm−20 mW laser with a 100× objective, resulting in the spot size of less than 2 μm.

All spectra exhibited features with bands indicative of hydrous, nanocrystalline $WO_3 \cdot xH_2O$.[48,49] The sharp peak at 960 cm^{-1} is attributed to the symmetric stretching mode of the terminal W═O bonds. The stretching modes of O−W−O for the bridging oxygens across planes, which occur around 660 cm^{-1} (with bending modes around 230 and 270 cm^{-1}), are expected from the layered and two-dimensional character of $WO_3 \cdot 2H_2O$. They are also suggested to be influenced significantly by hydration levels and the 660 cm^{-1} band is used for identifying the hydration level. The rest of the modes between 100 and 300 cm^{-1} are attributed to the lattice modes. As can be seen, two bands appear at 660 and 685 cm^{-1}, which indicate that the material is fully hydrated as $WO_3 \cdot 2H_2O$. For thin samples the intensity of all but the peaks at 660, 685, and 960 cm^{-1} decrease, asserting that only the strong planar modes survive as a result of thinning.

The annealing effect on Raman spectra has been presented in the Supporting Information. Following thermal annealing at 300 °C, the Raman spectral features of these platelets changed dramatically (Figure 4b), a sign of dehydration and formation of the monoclinic WO_3 (*m*-WO_3). As can be seen, two main regions for the *m*-WO_3 vibrations occur at 900−600 cm^{-1}, and below 300 cm^{-1}. The terminal W═O stretching mode at 960 cm^{-1} is now completely absent and the two peaks of 660 and 685 cm^{-1} have been replaced by two

(44) Chen, D. L.; Sugahara, Y. *Chem. Mater.* **2007**, *19*, 1808.
(45) Chen, D. L.; Gao, L.; Yasumori, A.; Kuroda, K.; Sugahara, Y. *Small* **2008**, *4*, 1813.
(46) Chemseddine, A.; Bloeck, U. *J. Solid State Chem.* **2008**, *181*, 2731.
(47) Rajeswari, J.; Kishore, P. S.; Viswanathan, B.; Varadarajan, T. K. *Nanoscale Res. Lett.* **2007**, *2*, 496.
(48) Daniel, M. F.; Desbat, B.; Lassegues, J. C.; Gerand, B.; Figlarz, M. *J. Solid State Chem.* **1987**, *67*, 235.
(49) Epifani, M.; Andreu, T.; Arbiol, J.; Diaz, R.; Siciliano, P.; Morante, J. R. *Chem. Mater.* **2009**, *21*, 5215.

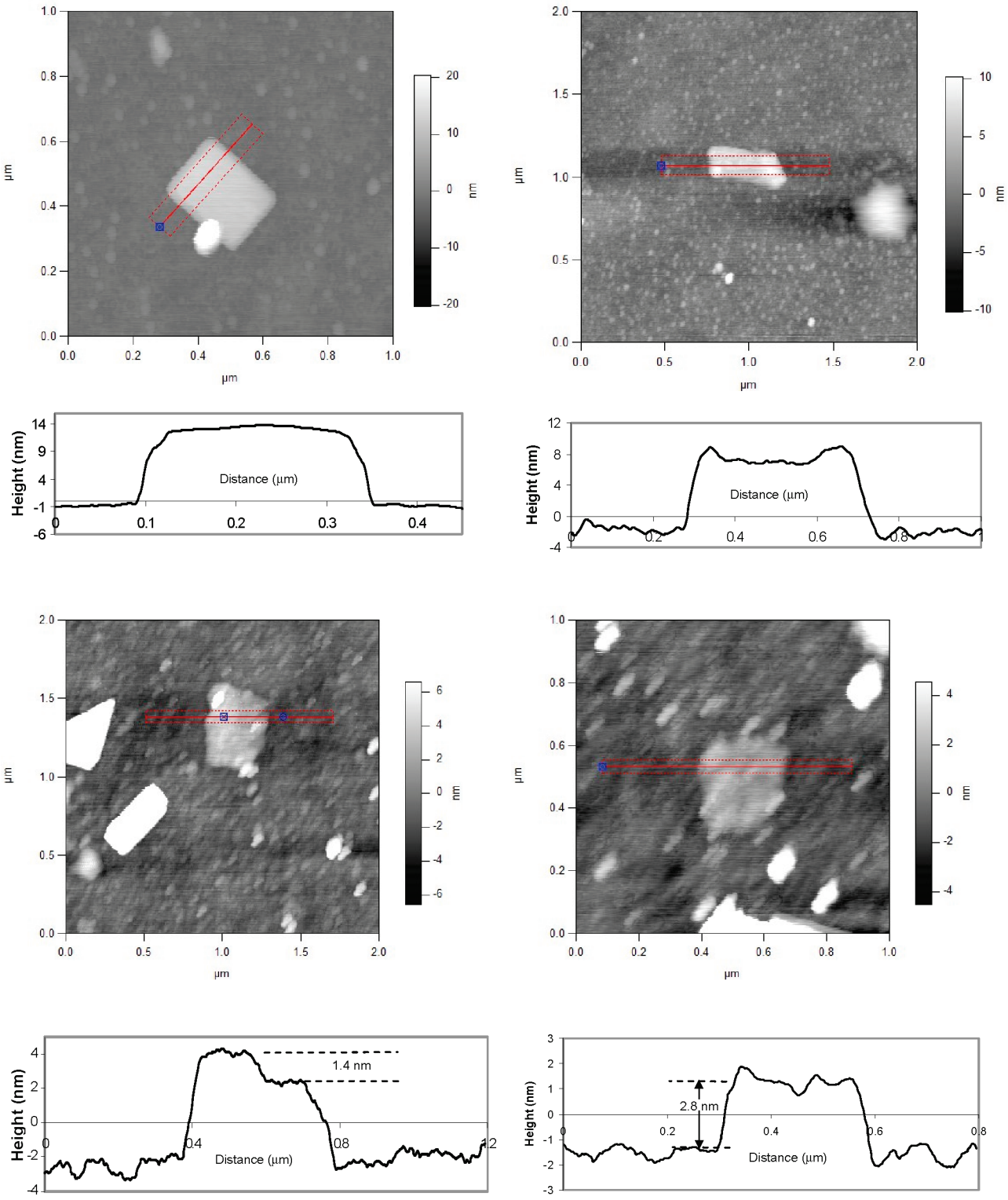

Figure 5. Typical AFM images and profiles of hydrated WO_3 sheets. Minimum thickness of 2.8 nm and a step height of 1.4 nm can observed. Roughness is caused by the surface quartz substrate surface.

strong bands at around 709 and 810 cm^{-1}. In addition to these, a strong peak appears at 272 cm^{-1} and two weaker peaks at 195 and 320 cm^{-1}. The peak that can be assigned to the shoulder seen at 690 cm^{-1} is typically associated with the presence of hexagonal WO_3.[50]

After thinning, the 272 cm^{-1} peak remains strong. However, both 190 and 320 cm^{-1} peaks which correspond to the vibration of the bending mode of W−O−W decreased rapidly. Additionally, the planar 709 and 810 cm^{-1} remain relatively strong, which is an indication of successful exfoliation process.

Atomic force microscopy (AFM) was carried out on hydrated layers on the substrates in order to assess their

(50) Balaji, S.; Albert, A. S.; Djaoued, Y.; Bruning, R. *J. Raman Spectrosc.* **2009**, *40*, 92.

thickness and to determine the minimum thickness of the thinnest exfoliated layers. An Asylum Research MFP-3D system was used for AFM imaging. As shown in Figure 5, for hydrated WO_3, a large number of sheets with 2−10 layers were resolved (with thicknesses of 2.8−14 nm). It seems that the mechanical exfoliation effectively separates layers at their weakest bonds, where they are held together by weak van der Waals forces.

Many sheets with a fundamental thickness of 2.8 nm appeared in profile measurements (Figure 5), essentially double that of $a = 1.380$ nm, which is approximately double the thickness of the unit cell for hydrated WO_3. It is possible that after the adhesion of the bottom layer onto the substrate, its surface energy alters so that it no longer favors the possible exfoliation of its adjacent top layer. However, the topmost layers are likely less affected by the substrate; hence, exfoliation of single stepped layers is achievable, with the thickness almost equal to $a = 1.380$ nm in the unit cell (Figure 5). Other thicknesses were observed to follow this quantized step of 1.4 nm and were all multiples of the unit cell parameter, a. On average, the observed steps were 2.8, 4.2, 5.6, 7 nm, etc., which correspond to multiples of unit cell sized steps. However very consistently after annealing, the layers' thicknesses decreased to half that of their hydrated counterparts (idealized crystal structures of both hydrated and annealed WO_3 are presented in the Supporting Information). After the evaporation of water molecules from the crystal lattice, the volume between WO_3 layers, once occupied by water molecules, decreases and the unit-cell height halves. The annealed WO_3 showed the steps of 0.7 nm, which corresponds to unit cells of monoclinic WO_3 without the water molecules.

To assess differences between thick and thin films, we carried out ion intercalation experiments. Intercalation of ions first occurs on the surface; hence, such experiments are a good indication of the exfoliation effect by distinguishing between thin and thick layers. Lithium intercalation was conducted using chemical reaction as suggested by Lee et al.[51] Pure lithium metal was evaporated onto the WO_3 platelets, which were exposed to the lithium metal flux at room temperature in a 1×10^{-5} mbar vacuum. The evaporated Li diffuses into the WO_3 to make bronze WO_3. Raman spectroscopy was used to show assess the effect of Li intercalation. As can be seen in Figure 6, only very thin plates (less than 10 nm) were affected by the exposure to Li for and thick flakes (more than 50 nm) Raman signatures remain largely intact. For very thin platelets the 705 cm^{-1} peak (shifted from 709 cm^{-1}) and its left side shoulder completely vanished, whereas the Li intercalation did not affect the thicker platelets. Lee et al. [52] suggested that the disappearance of the 705 cm^{-1} peak is due to increased vibrational symmetry along both axes after the Li intercalation. Results are in agreement with Lee et al.'s experiments.[51]

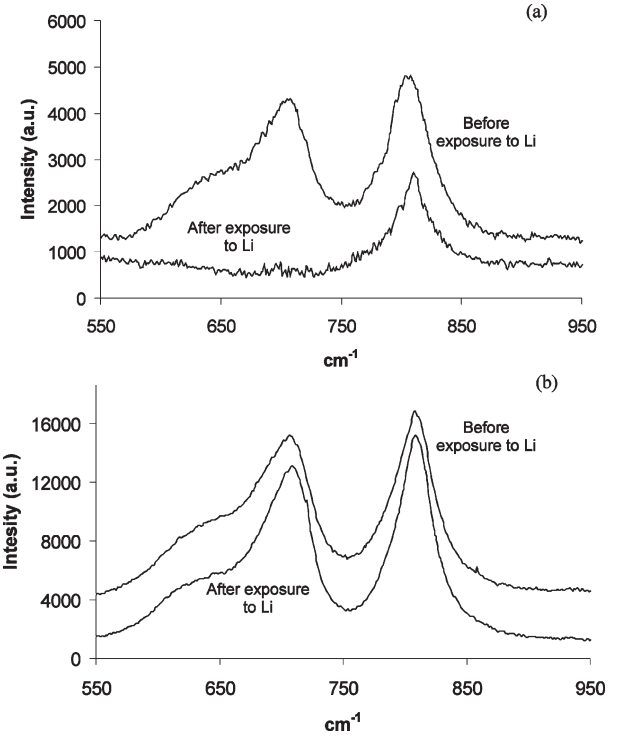

Figure 6. Effect of Li intercalation on Raman spectra of (a) thin and (b) thick sheets.

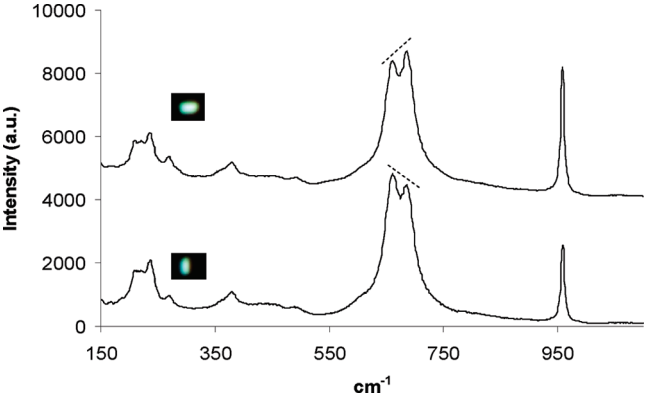

Figure 7. Effect of the growth directions along different unit-cell axes (a and b) on the planar O−W−O stretching modes intensities (inset figure width 2 μm).

The disappearance of the planar Raman peaks should be evaluated with care. In our experiments, it was observed that the planar direction of the growth significantly affects the intensity of peaks in the 600 to 900 cm^{-1} range, which are assigned to the planar O−W−O stretching modes. As can be seen in Figure 7, the growth with horizontal and vertical dominations result in the change in the relative intensity of different peaks of the hydrated WO_3. The same effect was also observed for the planar modes of the annealed WO_3 sheets with the different degrees of hydration. Not seeing shift any shifts for the 810 cm^{-1} peak can suggest that the intercalated Li ions dampen the 705 cm^{-1} stretching mode by affecting the WO_3 plane in one direction rather than making the system more symmetric. To further investigate the effect of reducing the thickness of the nanosheets on Raman

(51) Lee, S. H.; Liu, P.; Tracy, C. E.; Benson, D. K. *Electrochem. Solid-State Lett.* **1999**, *2*, 425.
(52) Lee, S. H.; Seong, M. J.; Cheong, H. M.; Ozkan, E.; Tracy, E. C.; Deb, S. K. *Solid State Ionics* **2003**, *156*, 447.

spectra after ion intercalation, the effect of Na^+ ion intercalation is presented in the Supporting Information.

Conclusion

We have shown the successful synthesis of atomically thin WO_3. These sheets have thicknesses that were multiples of the unit-cell height. Thinning of WO_3 can significantly affect physical and chemical behavior, which was demonstrated as significant Raman spectra changes after Li intercalation for thin samples.

The study of these atomically thin layers of WO_3 is paramount for understanding the effect of thinning to create 2D metal oxide sheets. Further investigation is required to understand the thinning effect on photon−electron and electron−photon interactions in these 2D structures. The suggested sheets can have great potential in developing 2D electronic and photonic devices for forming new generation of planar photodiodes and transistors. Such materials can be implemented for developing a wide variety of devices ranging from perfect insolating dielectric layers to layers with high mobility of carriers in 2D for creating transistors with large on−off ratios and transconductance. In addition, both the fabrication process and their framework have great compatibility with other emerging 2D materials such as graphene.[28]

Supporting Information Available: Annealing effect on Raman spectra, the effect of reducing the thickness of the nanosheets on Raman spectra after Na^+ ion intercalation, and the idealized crystal structure of the hydrated and annealed WO_3 double layers (PDF). This information is available free of charge via the Internet at http://pubs.acs.org/.